THE ASTRONOMICAL JOURNAL, 119:1695–1700, 2000 April

THE PARSEC-SCALE STRUCTURE AND EVOLUTION OF THE NEARBY FANAROFF-RILEY TYPE II RADIO GALAXY PICTOR A

S. J. TINGAY[1]
Jet Propulsion Laboratory, Mail Stop 238-331, California Institute of Technology, 4800 Oak Grove Drive, Pasadena, CA 91109; tingay@hyaa.jpl.nasa.gov
D. L. JAUNCEY, J. E. REYNOLDS, AND A. K. TZIOUMIS
Australia Telescope National Facility, CSIRO, P.O. Box 76, Epping, NSW 2121, Australia
P. M. MCCULLOCH, S. P. ELLINGSEN, AND M. E. COSTA
Department of Physics, University of Tasmania, G.P.O. Box 252C, Hobart, Tasmania 7001, Australia
J. E. J. LOVELL[2]
Institute of Space and Astronautical Science, Sagamihara, Kanagawa 229, Japan
R. A. PRESTON
Jet Propulsion Laboratory, Mail Stop 238-335, California Institute of Technology, 4800 Oak Grove Drive, Pasadena, CA 91109
AND
S. M. SIMKIN
Department of Physics and Astronomy, Michigan State University, East Lansing, MI 48824-1116
Received 1999 June 22; accepted 2000 January 4

ABSTRACT

We present very long baseline interferometry (VLBI) images of the core emission from a nearby bright FR II radio galaxy, Pictor A, revealing its parsec-scale jet structure and evolution for the first time. These data constitute a significant addition to our knowledge of powerful radio galaxies on the smallest scales, effectively doubling the number studied at this resolution. The jet, 14 h^{-1} pc in projected extent, is directed west of the core for the first 5 h^{-1} pc and then appears to bend approximately 40° to the north. Apparent motions for three of the five parsec-scale jet components have been estimated, 0.5 ± 0.4, 1.1 ± 0.5, and 0.4 ± 0.7 $h^{-1}c$, indicating that subluminal motion is likely. No parsec-scale counterjet has been detected, allowing only lower limits on the jet-to-counterjet surface brightness ratio to be estimated. Two models, one describing the apparent 40° bend in the parsec-scale jet as an intrinsic deflection of the jet and one describing it as the effect of jet precession, may each be plausible and should be testable with future VLBI observations. By adopting the jet deflection model to describe the apparent 40° bend, we estimate that the Pictor A jet is initially inclined to our line of sight by less than 51°. Comparing this result with VLBI observations of Cygnus A suggests that, while the components in both jets are consistent with at least mildly relativistic speeds, the Pictor A jet lies significantly closer to our line of sight than the Cygnus A jet. This conclusion is consistent with both the parsec-scale radio structures and the kiloparsec-scale orientations of the host galaxies as well as the "unified model" interpretation of the optical spectra from these two objects.

Key words: galaxies: active — galaxies: individual (Pictor A = PKS 0518−458) — galaxies: jets — galaxies: nuclei — radio continuum — techniques: interferometric

1. INTRODUCTION

Pictor A (PKS 0518−458) is one of the very few nearby ($z = 0.035$) FR II–type radio galaxies (Fanaroff & Riley 1974) with a core bright enough to study routinely using simple very long baseline interferometry (VLBI) techniques. While not as luminous as Cygnus A, the prototypical FR II radio galaxy, Pictor A lies well above the FR I/FR II luminosity break and is approximately 40% closer than Cygnus A, allowing a detailed high-resolution study of the parsec-scale structure and evolution in a powerful lobe-dominated radio galaxy, something that has been undertaken at length only for Cygnus A (Krichbaum et al. 1998; Sorathia et al. 1996; Bartel et al. 1995; Carilli, Bartel, & Diamond 1994).

Systematic observations of FR II–type galaxies, such as Pictor A and Cygnus A, are important for testing theories that unify extragalactic radio sources based upon the orientation of their relativistic jets. Since the jets of FR II–type sources are supposed to be more in the plane of the sky than directed along our line of sight, we should expect to find smaller apparent speeds in FR II jets than in core-dominated radio sources, in which the jets are supposed to be more aligned with our line of sight. Systematic studies are underway, primarily on samples of lobe-dominated quasars (e.g., Hough et al. 1999; Vermeulen et al. 1993; Hough & Readhead 1989; Zensus & Porcas 1987), and currently the observations are generally consistent with a fairly simple relativistic jet model and the unification of core-dominated and lobe-dominated quasars (Hough et al. 1999). It is important to add galaxies to these studies so that the statistics are unbiased by orientation (Pearson 1996).

Recently, both optical and radio investigations have revealed in detail the kiloparsec-scale structure of Pictor A. Perley, Röser, & Meisenheimer (1997) performed the first comprehensive study of Pictor A with the Very Large Array (VLA) over the wavelength range 2–400 cm. They find strong evidence that the extended optical emission of Pictor

[1] Current address: Paul Wild Observatory, Australia Telescope National Facility, CSIRO, Locked Bag 194, Narrabri, NSW 2390, Australia.
[2] Current address: Australia Telescope National Facility, CSIRO, c/o COSSA, G.P.O. Box 3023, Canberra, ACT 2601, Australia.

A (Röser & Meisenheimer 1987) is due to synchrotron emission from electrons reaccelerated in the western lobe hot spot. Simkin et al. (1999) have recently studied high-resolution optical images of the host galaxy obtained with the *Hubble Space Telescope* (*HST*). The images, combined with optical spectroscopy and radio images obtained with the Australia Telescope Compact Array (ATCA), provide evidence for significant disruption of the interstellar medium in the nuclear regions of the galaxy. Earlier ground-based optical observations of Pictor A have been reported by Filippenko (1985) and Carswell et al. (1984). Perley et al. (1997) also give a concise summary of other past observations from radio to X-ray bands.

With the large-scale structure of Pictor A relatively well studied, we turn to the small-scale structures in the source, those on parsec scales, which are best probed using VLBI techniques at radio wavelengths. Schilizzi (1976) was the first to estimate the flux density of the Pictor A nucleus at VLBI resolution, 0.9 Jy at 8.1 GHz. Using the 275 km Parkes-Tidbinbilla interferometer, Jones, McAdam, & Reynolds (1994) found a flux density of 1.1 Jy at 8.4 GHz and a spectral index between 2.3 and 8.4 GHz of -0.06 ($S \propto \nu^{\alpha}$). More recent flux density monitoring of the Pictor A nucleus with ATCA also shows a flat radio spectrum between 4.8 and 8.4 GHz and a flux density of approximately 1.2 Jy (Tingay et al. 2000). Thus, the high flux density and compactness of the radio nucleus and the proximity of Pictor A, coupled with the rarity and importance of VLBI observations of FR II radio galaxies, form the motivation behind our VLBI investigations.

In § 2, we describe Southern Hemisphere VLBI Experiment (SHEVE) and Very Long Baseline Array (VLBA) observations of Pictor A. In § 3, we discuss the results of these observations and compare Pictor A with the FR II radio galaxy most extensively studied with VLBI, Cygnus A.

2. OBSERVATIONS AND DATA REDUCTIONS

VLBI imaging observations of Pictor A were obtained using the SHEVE array (Preston et al. 1989; 1992; Jauncey et al. 1994), as listed in Table 1. The SHEVE data were recorded with the Mark II recording system using a 2 MHz bandwidth and correlated at the JPL/Caltech Block II processor. The correlated data were fringe-fitted using the Astronomical Image Processing System (AIPS)[3] task FRING. System temperature and gain information was collected from each telescope, and standard calibration routines in the Caltech VLBI reduction package (Pearson 1991) were used to apply them to the fringe-fitted data. The fringe-fitted and amplitude-calibrated data were edited, time-averaged, imaged, and model-fitted using the DIFMAP imaging software (Shepherd, Pearson, & Taylor 1994).

TABLE 1

OBSERVATION LOG FOR PICTOR A

Epoch	Frequency (GHz)	Participating Telescopes[a]
1991 Mar 12.....	2.291	Ds43, Pk, Hb, Na
1993 Jul 3.....	8.418	Ds43, Pk, Hb, Na, Mr, Pr15, Ht
1999 Mar 7.....	8.391	VLBA

[a] (Ds43) Tidbinbilla (70 m); (Pk) Parkes; (Hb) Hobart; (Na) Narrabri; (Mr) Mopra; (Pr15) Perth (15 m); (Ht) Hartebeesthoek; (VLBA) Mauna Kea, Saint Croix, Los Alamos, Fort Davis, Pie Town, Kitt Peak, and Owens Valley.

[3] The Astronomical Image Processing System was developed by the National Radio Astronomy Observatory, which is operated by Associated Universities, Inc., under cooperative agreement with the National Science Foundation.

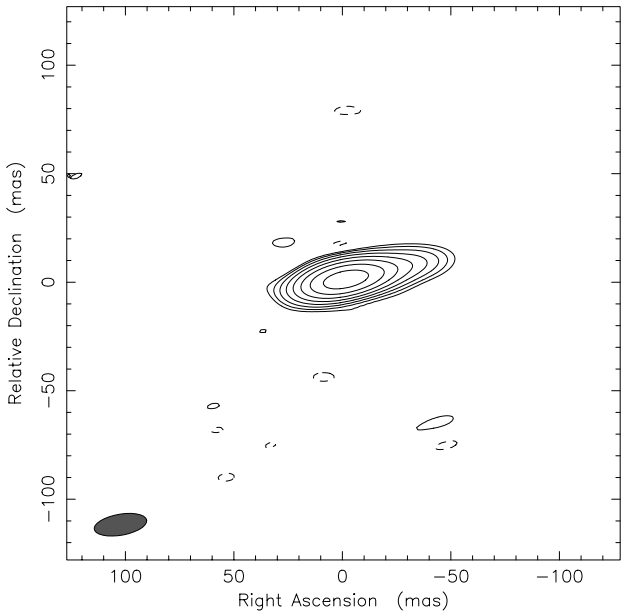

FIG. 1.—VLBI image of Pictor A at 2.291 GHz on 1991 March 12: map peak, 1.03 Jy beam^{-1}; contours, -0.5%, 0.5%, 1%, 2%, 4%, 8%, 16%, 32%, and 64% of peak; beam FWHM, 24.5 by 9.7 mas at $-80.^{\circ}0$.

VLBA observations of Pictor A were undertaken as listed in Table 1, using a 64 MHz bandwidth.[4] The data were correlated at the VLBA processor in Socorro and fringe-fitted and amplitude-calibrated in AIPS according to the standard procedure for continuum VLBI reductions listed in the AIPS Cookbook. The data were frequency-averaged in AIPS and exported to DIFMAP for editing, time averaging, imaging, and model fitting. Model fitting proceeded following Tingay et al. (1998), and all model-fitting components were Gaussian.

3. RESULTS AND DISCUSSION

Figure 1 shows the image produced from the 1991 SHEVE data at 2.291 GHz. At this frequency with this array, the source is only marginally resolved but is clearly extended toward the western lobe hot spot, in the same direction as the weak jet seen in VLA images (Perley et al. 1997).

Figure 2 shows the image produced from the 1993 SHEVE data at 8.418 GHz. In this higher resolution image, the jet is sufficiently resolved that a model has been fitted to the *u-v* data. Table 2 lists the model components fitted to the 1993 data, and the positions of the components are indicated on Figure 2.

In both Figure 1 and 2 the brightest and most compact feature lies at the southeast end of the source. This is the

[4] The Very Long Baseline Array is operated by the National Radio Astronomy Observatory.

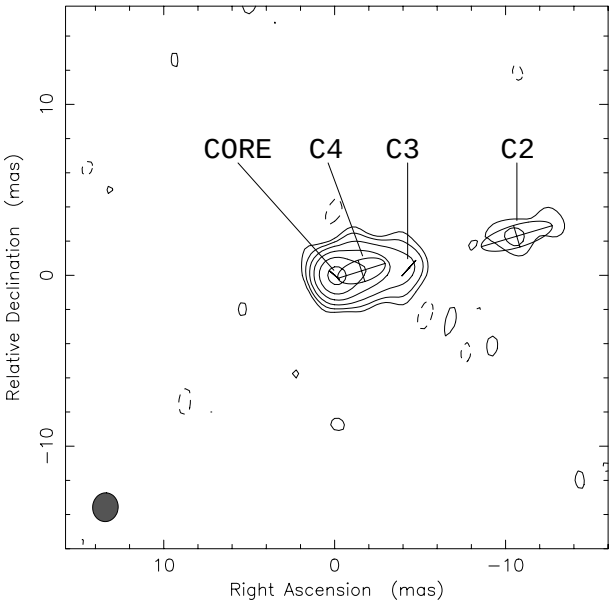

FIG. 2.—VLBI image of Pictor A at 8.418 GHz on 1993 July 3: map peak, 0.32 Jy beam^{-1}; contours, −2.5%, 2.5%, 5%, 10%, 20%, 40%, and 80% of peak; beam FWHM, 1.7 by 1.5 mas at −5°.1. Model components listed in Table 2 are overlaid on the image.

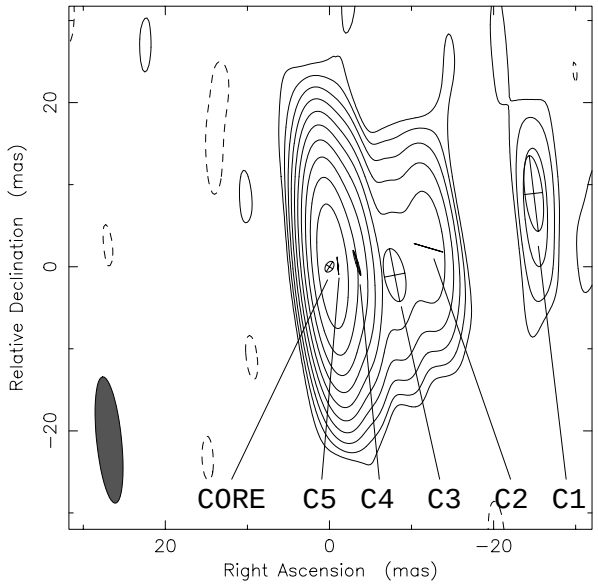

FIG. 3.—Short-baseline VLBI image of Pictor A at 8.391 GHz on 1999 March 7: map peak, 0.72 Jy beam^{-1}; contours, −0.1%, 0.1%, 0.2%, 0.4%, 0.8%, 1.6%, 3.2%, 6.4%, 12.8%, 25.6%, and 51.2% of peak; beam FWHM, 15.5 by 3.0 mas at 5°.8. Model components listed in Table 3 are overlaid on the image.

flattest spectrum component in the source, leading us to identify it as the active core.

Figure 3 is an image made from the short baselines of the 1999 VLBA observation at 8.391 GHz (including these antennas: Los Alamos, Fort Davis, Pie Town, Kitt Peak, and Owens Valley). The limited *u-v* coverage of the VLBA can be effectively used at this far southern declination, as the source is extended essentially in an east-west direction. Again a model has been fitted to the *u-v* data. The model is listed in Table 3 and the positions of the components are indicated on Figure 3.

The 1999 VLBA observation was more sensitive than the 1993 SHEVE observation, and an extra component approximately 26 mas from the core can be seen in Figure 3 and Table 3. The 1993 observations were not sensitive enough to detect this faint component, and the 1991 observations were too low-resolution to resolve it.

Based on the model-fitting of the 1993 and 1999 data, the simplest identification of components from epoch to epoch is indicated in Figures 2, 3, and 4. Five jet components were detected in Figure 3 and three jet components were detected in Figure 2. This difference can be most simply explained by the following two reasonable statements: First, the component C5, detected close to the core in 1999 (Figs. 3–4), was not detected 5.6 yr earlier (Fig. 2) because it had not been ejected from the core far enough to be resolved. Second, the component C1, detected far from the core in 1999 (Fig. 3), was not detected 5.6 yr earlier (Fig. 2) because of a combination of resolution and sensitivity effects. Allowing for the innermost and outermost components detected in Figure 3 leaves the three components between approximately 2 and 12 mas at both epochs to be plausibly identified with each other, since each appears farther from the core in 1999 than in 1993.

Figure 4 shows an image, also produced from the 1999 VLBA data but using the full range of VLBA baselines available. This higher resolution image shows an excellent correspondence with the model of Table 3, with the exception of component C1, which is resolved out in Figure 4.

TABLE 2

MODEL COMPONENTS FITTED TO THE 1993 SHEVE DATA AT 8.418 GHz

Component (1)	S (Jy) (2)	d (mas) (3)	θ (deg) (4)	A (mas) (5)	B/A (6)	ϕ (deg) (7)
Core.....	0.28	0.00	0.0	0.73	0.00	48.9
C4	0.36	1.59	−80.6	2.90	0.45	−72.5
C3	0.03	4.36	−84.4	1.21	0.00	−41.8
C2	0.05	10.90	−77.9	4.32	0.30	−73.5

NOTES.—Col. (2): Integrated flux density of the model component. Col. (3): Distance of the model component from the designated phase center. Col. (4): Position angle of the model component centroid from the designated phase center in degrees east of north. Col. (5): Length of the major axis of the model component. Col. (6): Ratio of model component minor axis to major axis. Col. (7): Position angle of the model component major axis in degrees east of north.

3.1. *A Deflected or Precessing Parsec-Scale Jet?*

When considering the VLBI images, the first point of note is that the parsec-scale jet of Pictor A appears to undergo a significant apparent bend approximately 10 mas

TABLE 3

MODEL COMPONENTS FITTED TO THE 1999 VLBA DATA AT 8.391 GHz

Component (1)	S (Jy) (2)	d (mas) (3)	θ (deg) (4)	A (mas) (5)	B/A (6)	ϕ (deg) (7)
Core.....	0.59	0.00	0.0	1.44	0.65	−32.7
C5	0.20	1.03	−84.1	2.13	0.00	5.3
C4	0.12	3.38	−81.9	3.17	0.09	16.8
C3	0.02	8.01	−97.3	6.56	0.39	11.0
C2	0.03	12.29	−79.2	3.62	0.00	73.6
C1	0.01	26.45	−70.3	9.28	0.23	6.8

NOTE.—Columns same as in Table 1.

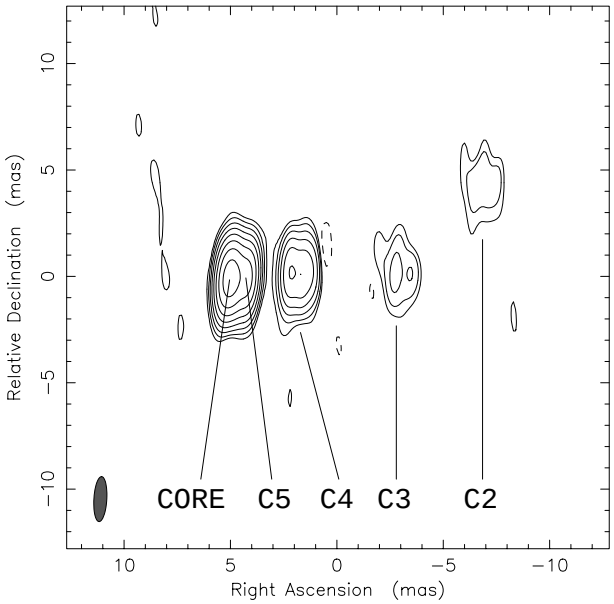

FIG. 4.—Long-baseline VLBI image of Pictor A at 8.391 GHz on 1999 March 7: map peak, 0.40 Jy beam^{-1}; contours, −0.5%, 0.5%, 1%, 2%, 4%, 8%, 16%, 32%, and 64% of peak; beam FWHM, 2.1 by 0.6 mas at −3°.4. The data and model have been shifted by (5, 0) mas.

(5 h^{-1} pc) from the core, especially apparent at high resolution in Figure 4, between the positions of components C2 and C3. Initially the parsec-scale jet appears to travel to the west for approximately 10 mas and then experiences an approximately 40° apparent bend. A hint of this apparent bend can also be seen in Figure 2. It is easier to identify in Figures 3–4 because the jet is detected farther from the core and because the components have moved farther from the core since 1993. From Figure 3 it appears that the faint component C1 lies at a position angle of −70° relative to the core. Farther from the core, the *HST* continuum images of Simkin et al. (1999) show a possible subarcsecond-scale optical jet on a scale of 150 mas, also at a position angle of −70°. Finally, from a 20 cm VLA observation the jet appears to travel along a position angle of −78° between 7″.5 (the resolution of the VLA observation) and 180″ and then bend slightly to travel the remaining distance to the lobe at a position angle of −85° (Perley et al. 1997). This arcsecond-scale jet is faint and difficult to differentiate from the background lobe emission (Perley et al. 1997).

If the apparent 40° bend in the parsec-scale jet is attributable to a single intrinsic bend in the jet, then significant projection effects are required. Using a simple model that describes mild bends in relativistic jets as deflections caused by single oblique shocks, Tingay (1997) showed that the largest intrinsic bend possible in such a jet is 30°. If the intrinsic bend in the Pictor A jet is 30°, at the upper limit of consistency with this model, an initial jet angle to our line of sight (before the bend) of less than 51° is required to produce the apparent 40° bend that we observe (see eq. [1] in Conway & Murphy 1993).[5] Thus, using the jet deflection model, we estimate that the jet angle to our line of sight, within 10 mas of the core, is less than 51°.

We note a problem with the jet deflection hypothesis, however. An intrinsic bend in the jet of order 30° would mean that the jet direction at component C3 no longer points toward the western lobe hot spot. To realign the jet and the hot spot under this model could require additional deflections of the jet downstream of component C3 but closer to the core than 150 mas, since the *HST* images show the optical jet aligned with the VLA jet and the western hot spot on these scales. High-resolution, high-sensitivity VLBI observations at 2.3 GHz or a lower frequency to resolve the structure shown in Figure 1 would be required to explore this suggestion.

An alternative explanation for the apparent bend in the parsec-scale jet is jet precession. The position angles of the various features in the jet as a function of distance from the core then represent the time-history of the jet ejection axis, assuming that the discrete features we see in the radio images are moving ballistically. Under this hypothesis, the VLBI data suggest that the jet ejection axis has remained stable from 1986 to 1999, i.e., the component C3 was ejected in approximately 1986 (see § 3.2 for a discussion of the apparent motions of components C2, C3, and C4) and since then the components C4 and C5 have been ejected from the core and appear to have followed the trajectory of C3, along position angle −90° (Fig. 4). Before 1986 the components C1 and C2 appear to have been ejected along position angles −70° and −78°, respectively (Tables 3 and 2, respectively), consistent with the position angle of the optical jet suggested by Simkin et al. (1999). For component C2 we estimate an ejection date of approximately 1948, 38 yr before the ejection of C3, by virtue of its apparently lower speed.

These estimates suggest an approximately 10° projected change in the jet ejection direction over a period of approximately 38 yr, between the ejection dates of C2 and C3, and a further 10° projected change between the ejection dates of C1 and C2, though we cannot estimate what the time difference is, in this case. If this rate of projected directional change is applicable to the rest of the jet at later times, then we should expect that the position angles of components C3, C4, and C5 would be affected by precession also. From Figure 4 we see no discernible change in the jet position angle after the ejection of component C3. However, we might expect the total change in position angle between C3 and C5 to be only 3°–4° since 1986 (corresponding to the projected directional rate of change estimated above), which is below the limit discernible from the data, given that component C5 is barely resolved from the core component, even in Figure 4.

However, we need to note a difficulty with the precession model, again related to the large-scale morphology of Pictor A. If the jet has precessed at least over the limits in position angle suggested by the VLBI data, −70° to −90°, as rapidly as inferred above, on timescales of less than 100 yr, and over the lifetime of the source, then one might expect quite a different lobe and hot-spot structure than is seen with the VLA at 20 cm, for example (Perley et al. 1997). Pictor A has a bright and compact western hot spot at position angle −80° and no hint of recent or ancient hot spot activity at position angles close to −70° or −90°, within or without the highly symmetric western lobe, which is smooth in both intensity and spectral index distributions

[5] At the 51° inclination angle limit, an azimuthal angle (ϕ in Conway & Murphy 1993, eq. [1]) of approximately 115° is required for the jet following the bend; a wider range of azimuthal angles is possible as the initial inclination angle decreases from 51°. The maximum initial inclination angle of 51° is reduced if the intrinsic bend in the jet is less than 30°.

(Perley et al. 1997). In short, if we attribute the apparent parsec-scale jet bending to precession, which affects the jet all the way to the western hot spot, we may expect a much more complex hot-spot/lobe structure than has been observed with the VLA.

In our view, both the jet deflection model and a precessing-jet hypothesis may remain possible explanations for the parsec-scale structure of Pictor A, although both models have difficulties when the current body of VLBI, *HST*, and VLA data is considered. Happily, it seems that we may be able to resolve these difficulties and decide between these two models easily with future VLBI observations. If the precession hypothesis is correct, we will observe future components being ejected from the core with different position angles from the existing components and we will see the existing components continue along the position angles that they currently occupy. If the deflection hypothesis is correct, we would expect to see new components ejected at a constant position angle of $-90°$ and perhaps the existing components C3, C4, and C5 follow C2 through a similar bend a distance 10 mas from the core. Given the current angular speeds of these components, we should be able to distinguish between jet deflection and precession within about 10 yr.

In the remaining sections, we concentrate on the jet deflection model, since we believe that this provides the simpler of the two explanations for the current VLBI data and because this model provides a predicted upper limit on the jet inclination of 51°, which can be usefully compared with other optical observations of the Pictor A host galaxy and Cygnus A VLBI data.

3.2. *Parsec-Scale Component Motions*

Our simple identification of the parsec-scale jet components is partly based on the proposal that C2, C3, and C4 have consistently moved away from the core over the course of the 5.6 yr between observations. By comparing the positions of the components in the parsec-scale jet of Pictor A, between 1993 and 1999, both from the positions of the model-fitted components in Tables 2 and 3 and the component centroids from Figure 4, we have estimated the apparent speeds for these three parsec-scale jet components and listed them in Table 4.

The errors on the positions of the components were estimated at both epochs as the average of the half-width at half-maximum (HWHM) of the Gaussian components fitted to the data along the direction of component motion and the HWHM of the imaging restoring beams (see Figs. 2–4 for the 1993 and 1999 data), again measured along the direction of component motion. The positional errors at each epoch account for the quoted errors on the apparent speeds listed in Table 4.

TABLE 4

APPARENT SPEEDS OF COMPONENTS IN THE PICTOR A PARSEC-SCALE JET

Component (1)	D_{1993} (mas) (2)	D_{1999} (mas) (3)	ΔD (mas) (4)	$\beta_{app}h$ (5)
Core.....	...	...	...	...
C5	...	1.0 ± 0.8	...	...
C4	1.6 ± 1.0	3.4 ± 0.5	1.8 ± 1.5	0.5 ± 0.4
C3	4.4 ± 0.8	8.0 ± 0.9	3.6 ± 1.7	1.1 ± 0.5
C2	10.9 ± 1.4	12.3 ± 0.9	1.4 ± 2.3	0.4 ± 0.7
C1	...	26.4 ± 2.1	...	...

NOTES.—Col. (2): Component distance from the core at the 1993 epoch. Col. (3): Component distance from the core at the 1999 epoch. Col. (4): Difference between D_{1993} and D_{1999}. Col. (5): Apparent speed as a fraction of the speed of light ($H_0 = 100\ h$).

The component C5 is detected only in 1999 (Fig. 4 and Table 2) and was probably ejected from the core between 1993 and 1999 ($\sim$1996 if the mean of the apparent motions of C2, C3, and C4 is assumed for C5), allowing no estimate for its apparent speed. The component C1 was detected only in the lowest resolution 8.4 GHz image from 1999, as discussed above, again allowing no estimate of its apparent speed.

Using the maximum initial inclination angle of 51°, estimated above, we can place limits on the true speed of the components C3 and C4, the two components that lie along the initial jet direction, closer to the core than the bend at 10 mas. Using the standard formulae (Pearson & Zensus 1987), $h = 1$, and the apparent speeds with error bars from Table 4, the absolute minimum true speeds for components C3 and C4 are about $0.5c$ and about $0.1c$, respectively. These limits correspond to the lower limits in apparent speed for C3 and C4. The minimum true speeds corresponding to the best-fit apparent speeds of C3 and C4 are about $0.7c$ and about $0.5c$, respectively.

3.3. *Limits on a Parsec-Scale Counterjet*

No parsec-scale counterjet has been detected in Pictor A at 2.3 or 8.4 GHz, and we can only estimate lower limits for the jet-to-counterjet surface brightness ratio, R, at 8.4 GHz, from the 1999 observations. We estimate R by comparing the peak jet brightness at the positions of the components well resolved from the core, C1, C2, and C3 in Figure 3, with the peak positive off-source noise in Figure 3. These limits are the following: for C1, $R > 6$, for C2, $R > 23$, and for C3, $R > 27$.

Using the upper limit for the jet inclination of 51°, estimated from the jet deflection model, and lower limits on the true speeds, estimated from the best-fit apparent speeds for C3 and C4, we calculate a lower limit on the jet-to-counterjet surface brightness ratio of $R \gtrsim 1.5$ (assuming a continuous, flat-spectrum jet), much lower than measured. This result indicates that a combination of the following effects are likely: the jet is closer to the line of sight than 51°; the true component speeds are greater than the minimum values we have calculated; or the apparent motions of the components we observe are not indicative of the speed of the underlying jet.

3.4. *Comparison with Cygnus A*

Pictor A is a closer and less luminous version of Cygnus A, the prototypical FR II radio galaxy. On the parsec scale at 5 GHz, Cygnus A reveals a counterjet with $R = 5 \pm 2$ and component apparent motions of $\beta_{app} = 0.35 \pm 0.15\ h^{-1}$ (J1) and $\beta_{app} = 0.55 \pm 0.15\ h^{-1}$ (J4) (Sorathia et al. 1996; Bartel et al. 1995). When used as constraints on the beaming equations, these measurements have been used as evidence that the value of H_0 must be closer to 50 than 100, so that the Cygnus A jet lies at an angle to our line of sight away from the quasar–radio galaxy transition angle of 44°.4 proposed by Barthel (1989) and appears as a galaxy, not a quasar (Carilli et al. 1996).

Krichbaum et al. (1998), using 22 GHz VLBI images, find a range of apparent speeds in the Cygnus A jet between $0.1c$

and 0.7c, indicating a possible acceleration of components after they pass beyond 1 mas of the core, and a jet-to-counterjet surface brightness ratio close to unity at 1.6 and 43 GHz. Krichbaum et al. (1998) model the frequency dependence of R between 1.6 and 43 GHz with a partially obscuring free-free absorbing torus and infer true jet speeds of greater than 0.2 hc and a jet angle to our line of sight of more than 80°.

Thus, it appears that both Pictor A and Cygnus A have at least mildly relativistic component speeds, while neither is significantly superluminal, indicating that both jets lie away from our line of sight. However, from the estimates of jet inclination angle for both sources, it appears that the Pictor A jet (at least initially) lies closer to our line of sight ($\theta < 51°$ from the jet deflection model discussed above) than the Cygnus A jet ($50° < \theta < 85°$ using $h = 0.5$ to avoid the quasar–radio galaxy transition angle 44°.4). This is consistent with what we know about the parsec-scale counterjets in these two sources. Cygnus A has a strong counterjet, $R < 5$, whereas the lower limits on the Pictor A counterjet are higher, indicating that Cygnus A is likely to lie closer to the plane of the sky than Pictor A.

The inferred orientation of the radio jets for these two FR II objects is also consistent with what is known about the large-scale optical properties of their host galaxies and the optical active galactic nucleus version of the "unified model" (Antonucci 1993; Urry & Padovani 1995). Although the kinematics of the nonnuclear, optical emission-line gas in these two radio galaxy hosts is complex and clearly shows nonequilibrium components (Tadhunter, Metz, & Robinson 1994; Ridgway & Stockton 1997; Simkin et al. 1999), the global gas motions can be interpreted as arising from clouds in orbit around an axis that lies nearly in the plane of the sky (85°–90°) for Cygnus A (Simkin 1977) and an axis that is closer to our line of sight for Pictor A (Simkin & Callcut 1996; Simkin et al. 1999). This suggests that the radio jet axis and the rotation axis of the gas in the host galaxies have similar orientations (Baum, Heckman, & Van Breugel 1992). In addition, the nuclear emission lines from these two objects place Cygnus A, with a narrow-line optical spectrum (Tadhunter et al. 1994), in the narrow-line radio galaxy class, comparable to Seyfert 2 galaxies, and place Pictor A, with broad, variable nuclear emission lines (Sulentic et al. 1995; Halpern & Eracleous 1994; Filippenko 1985; Carswell et al. 1984), in the broad-line radio galaxy class, comparable to Seyfert 1 galaxies. These similarities suggest that Pictor A may lie close to or below the quasar–radio galaxy transition angle and that we are seeing farther past the obscuring nuclear torus in the optical for Pictor A than Cygnus A.

4. SUMMARY

We have imaged the radio nucleus of Pictor A, a nearby FR II radio galaxy, for the first time, revealing its parsec-scale structure and evolution at 2.3 and 8.4 GHz by measuring the source morphology and component motions. Using a model for deflections of a relativistic jet, we suggest that the Pictor A jet is initially inclined to our line of sight at an angle less than 51° and that the true speeds of components in the jet are likely to be at least mildly relativistic. A comparison of the VLBI data for Pictor A and Cygnus A leads us to suggest that, while both sources are consistent with at least mildly relativistic component speeds, the Pictor A jet probably lies closer to our line of sight than the Cygnus A jet, at least on the parsec scale. This is qualitatively consistent with both optical observations of the host galaxy kinematics and broad optical emission lines from the Pictor A nucleus.

We would like to thank the appointed referee, who suggested that we explore the alternative precession model for the parsec-scale jet bending and made other useful comments on the manuscript. Part of this work was carried out while S. J. T. held an NRC-JPL/NASA Research Associateship. Part of this research was carried out at the Jet Propulsion Laboratory, California Institute of Technology, under contract with the US National Aeronautics and Space Administration. The Australia Telescope is funded by the Commonwealth of Australia for operation as a National Facility managed by CSIRO.

REFERENCES

Antonucci, R. R. J. 1993, ARA&A, 31, 473
Bartel, N., Sorathia, B., Bietenholz, M., Carilli, C., & Diamond, P. 1995, Proc. Natl. Acad. Sci., 92, 11371
Barthel, P. D. 1989, ApJ, 336, 606
Baum, S. A., Heckman, T. M., & van Breugel, W. 1992, ApJ, 389, 208
Carilli, C. L., Bartel, N., & Diamond, P. 1994, AJ, 108, 64
Carilli, C. L., Perley, R. A., Bartel, N., & Sorathia, B. 1996, in ASP Conf. Ser. 100, Energy Transport in Radio Galaxies and Quasars, ed. P. E. Hardee, A. H. Bridle, & J. A. Zensus (San Francisco: ASP), 287
Carswell, R. F., Baldwin, J. A., Atwood, B., & Phillips, M. M. 1984, ApJ, 286, 464
Conway, J. E., & Murphy, D. W. 1993, ApJ, 411, 89
Fanaroff, B. L., & Riley, J. M. 1974, MNRAS, 167, 31P
Filippenko, A. V. 1985, ApJ, 289, 475
Halpern, J. P., & Eracleous, M. 1994, ApJ, 433, L17
Hough, D. L., & Readhead, A. C. S. 1989, AJ, 98, 1208
Hough, D. H., et al. 1999, ApJ, 511, 84
Jauncey, D. L., et al. 1994, in IAU Symp. 158, Very High Angular Resolution Imaging, ed. J. G. Robertson & W. G. Tango (Dordrecht: Kluwer), 13
Jones, P. A., McAdam, W. B., & Reynolds, J. E. 1994, MNRAS, 268, 602
Krichbaum, T. P., Alef, W., Witzel, A., Zensus, J. A., Booth, R. S., Greve, A., & Rogers, A. E. E. 1998, A&A, 329, 873
Pearson, T. J. 1991, BAAS, 23, 991
———. 1996, in ASP Conf. Ser. 100, Energy Transport in Radio Galaxies and Quasars, ed. P. E. Hardee, A. H. Bridle, & J. A. Zensus (San Francisco: ASP), 97
Pearson, T. J., & Zensus, J. A. 1987, in Superluminal Radio Sources, ed. T. J. Pearson & J. A. Zensus (Cambridge: Cambridge Univ. Press), 1
Perley, R. A., Röser, H.-J., & Meisenheimer, K. 1997, A&A, 328, 12
Preston, R. A., et al. 1989, AJ, 98, 1
———. 1993, in Sub-Arcsecond Radio Astronomy, ed. R. J. Davis & R. S. Booth (Cambridge: Cambridge Univ. Press), 428
Ridgway, S. E., & Stockton, A. 1997, AJ, 114, 511
Röser, H.-J., & Meisenheimer, K. 1987, ApJ, 314, 70
Schilizzi, R. T. 1976, AJ, 81, 946
Shepherd, M. C., Pearson, T. J., & Taylor, G. B. 1994, BAAS, 26, 987
Simkin, S. M. 1977, ApJ, 217, 45
Simkin, S. M., & Callcut, J. 1996, in Cygnus A: Study of a Radio Galaxy, ed. C. L. Carilli & D. E. Harris (Cambridge: Cambridge Univ. Press)
Simkin, S. M., Sadler, E. M., Sault, R., Tingay, S., & Callcut, J. 1999, ApJS, 123, 447
Sorathia, B., Bartel, N., Bietenholz, M., & Carilli, C. 1996, in Cygnus A: Study of a Radio Galaxy, ed. C. L. Carilli & D. E. Harris (Cambridge: Cambridge Univ. Press), 86
Sulentic, J. W., Marziani, P., Zwitter, T., & Calvani, M. 1995, ApJ, 438, L1
Tadhunter, C. N., Metz, S., & Robinson, A. 1994, MNRAS, 268, 989
Tingay, S. J. 1997, A&A, 327, 550
Tingay, S. J., et al. 2000, in preparation
———. 1998, AJ, 115, 960
Urry, C. M., & Padovani, P. 1995, PASP, 107, 803
Vermeulen, R. C., Bernstein, R. A., Hough, D. H., & Readhead, A. C. S. 1993, ApJ, 417, 541
Zensus, J. A., & Porcas, R. W. 1987, in Superluminal Radio Sources, ed. T. J. Pearson & J. A. Zensus (Cambridge: Cambridge Univ. Press), 126